1 EXECUTIVE SUMMARY

This report describes in detail a quadcopter which has been designed by the Penn State Autonomous Robotics Competition Club (ARCC) to compete in the 2nd VFS DBF competition. This year's challenge involves the development of a vertical take-off and landing (VTOL) vehicle capable of carrying a payload around the course shown in Figure 1. The pilot (flight control software in case of autonomous flight) must perform a full VTOL landing inside each one of the three landing zones for the lap to be deemed successful. The *flight performance* challenge involves flying as many laps as possible carrying a payload (minimum 2lb) within 10 minutes. This challenge allows a certified team member to pilot the vehicle. The autonomy course on the other hand, requires a single lap of the course be flown without human intervention.

To design such a vehicle, we first considered the various VTOL configurations and the factors that would maximize the score as defined by the organizers. Payload capacity, flight speed, 10 minutes of flight time, ease of control, and autonomy were design drivers arising from the competition rules. Low cost, ease of manufacture, maintainability, and availability of suitable components were requirements that arose from economic and technical concerns specific to our team. Based on these design drivers, the configuration and components were weighted with an X-quadcopter configuration being identified as the most suitable platform.

CAD was used to design the vehicle and simulate its structural integrity and estimate its aerodynamic drag. A mission model was developed to estimate competition performance such as number of laps completed, flight time, and endurance. These parameters were iterated upon to estimate required powertrain numbers. A suitable power train and associated control electronics were procured off the shelf with a combination of CNC machined aluminum frame parts, carbon fiber (CF) tubes, and 3D printed components being used to fabricate the structure. The assembled vehicle weighing in at 4.4Kg including a 1.81 (4 lb.) payload is shown in Figure 2.

Figure 2: X-Quadcopter build for DBF competition

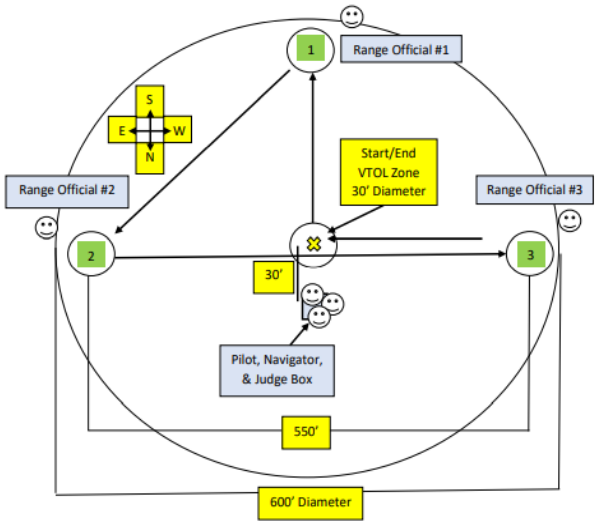

Figure 1: Course layout as shown in the request for proposal [4]

The physical vehicle was manually piloted, and the performance numbers were compared to our theoretical estimates. We found that we under-estimated the total flight time which was far more than the 10-minute limit. This allows us to increase the payload if desired to improve our score in the competition. Structurally this would be acceptable due to the safety factors used in the structural design. We plan to continue autonomous flight testing and tuning along with manual pilot training until the competition to maximize our chance of winning.

2 PROJECT SUMMARY

2.1 TEAM OVERVIEW

The team primarily is made up of 4 members from ARCC: Ghanghoon Paik, Rachel Axten, Ramona Devi, and Vidullan Surendran. The responsibilities taken on by each member are shown in Table 1.

Table 1:Primary responsibilities assigned to each team member

Vidullan Surendran (Point of contact)	Ghanghoon Paik	Ramona Devi	Rachel Axten
CAD modelling FEA and CFD Fabrication of components System Integration Documentation	Trajectory optimization Preliminary structural analysis Software development Documentation Fabrication of components	PID Tuning Ground station setup Flight plan setup Documentation	Certified safety Pilot Flight testing

2.2 SCHEDULE

A detailed schedule of the project is shown in Figure 3. Items marked in green have been completed, items in yellow are in progress, whereas items in red are behind schedule. The subsystem primarily affected by each task is also highlighted in the chart with *C* referring to computation/autonomy, *E* to electrical subsystems, *P* to the powertrain, *S* to structures, and *M* to overall management. Currently, we have a completed drone which is being flown manually and autonomous successfully.

Due to the restrictions on using non-US based components imposed upon the teams by ARL, major changes to the electronics architecture affecting autonomy were required after ARL review. The autonomous flight capabilities are currently being retested to ensure safe operation with a reduced sensor load and the team has fallen behind schedule on this task (marked in red). We continue to conduct manual test flights to improve pilot skills and fine tune the PID controllers onboard for improved stability in addition to testing the autonomous flight mode. Pilot training has been identified as a key priority as personnel skill is one of the largest factors affecting competition performance.

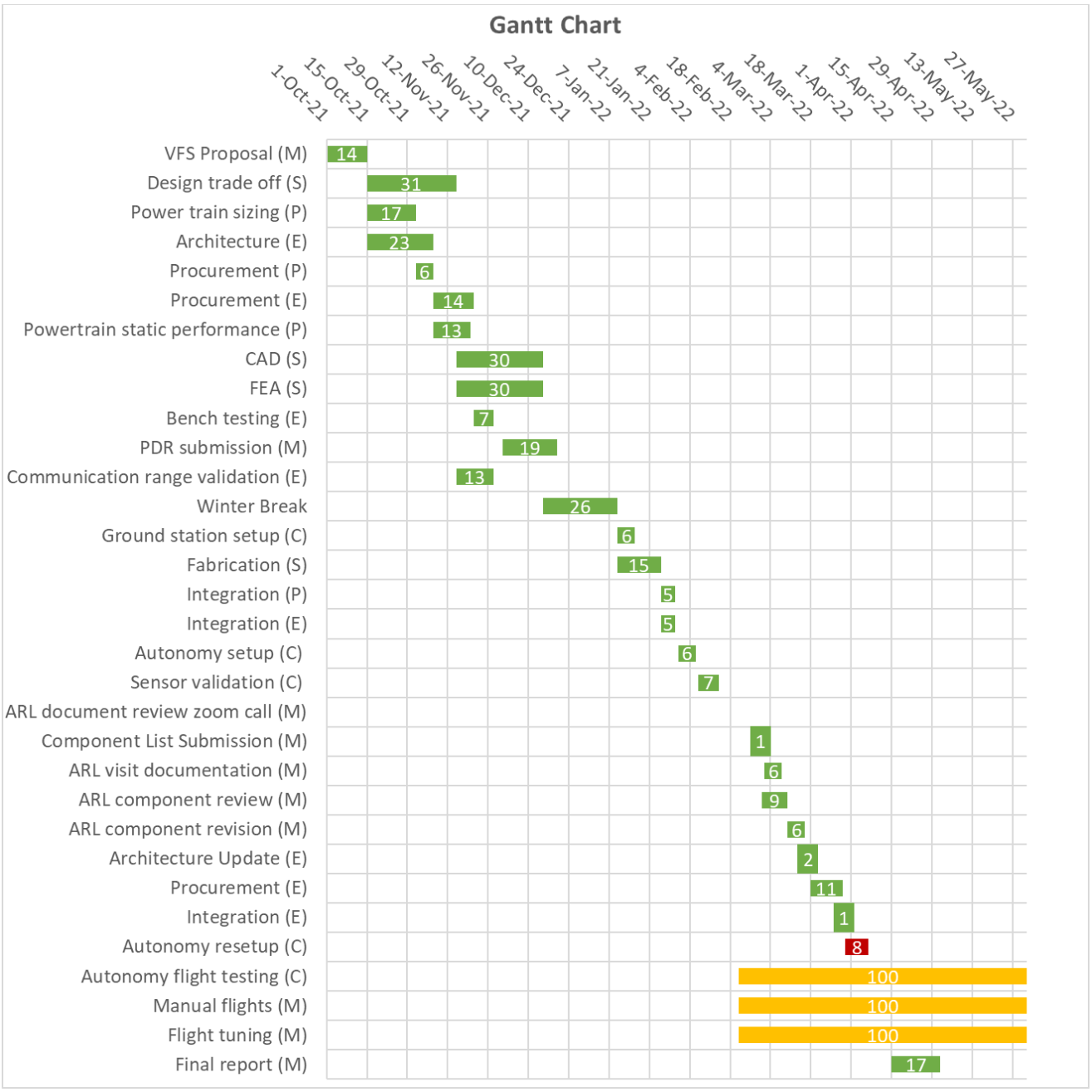

Figure 3 Schedule of project. Chart Key: (E) Electrical, (P) Propulsion, (S) Structures, (C) Coding/Autonomy, (M) Executive

3 Design Trade Studies

3.1 Mission Requirements

The two challenges and the safety requirements enforced by the organizers were decomposed into high level requirements shown in Table 2. The competition enforces a minimum payload requirement (2.1A) which we superseded with a 4lb payload requirement (2.1B).

Table 2: Requirements

ID	Requirement	Affected subsystems	Importance
	Safety		
1.1	Battery cannot exceed 6 cells in series	Electrical, Propulsion	Mandatory
1.2	Fuse in-line with each battery	Electrical	
1.3	Each propulsion battery must be identical	Electrical	
1.4	Separate power source for flight controls	Electrical	
1.5	Kill switch on radio transmitter	Electrical	
1.6	Shunt switch or similar yank switch 6 inches from propeller blades for emergency stop	Electrical, Structures	
1.7	Each battery must be under 100 W-h	Electrical	
1.8	Must use FCC approved radio bands	Electrical	
1.9	Congress/DoD approved electronic components	Electrical	
	Mission Specific		
2.1A	2Lb payload capacity (minimum)	Propulsion, Structures	Mandatory
2.2	All-up weight incl. payload (AUW) under 15lbs	All subsystems	
2.3	End-to-end dimension under 1980mm	Structures, Propulsion	
2.4	Vertical takeoff and landing	Propulsion, Structures	
2.5	Manually controlled FPV flight	Electrical, Controls	
2.1B	4Lb of payload capacity	Propulsion, Structures	Optional
2.6	10 minutes of flight time at 75% throttle	Electrical, Propulsion	
2.7	Autonomy assisted manual flight	Controls, Electrical	
2.8	Level 3 autonomy for autonomy challenge: Localization using GPS and waypoint control	Electrical, Controls	
2.9	Capable of 15 endurance laps	Propulsion, Electrical	
2.10	Forward flight max of at least 8 m/s	Propulsion, Structures	

3.2 Design Drivers

Many requirements affect multiple subsystems and trade-offs are required. For example, an increase in power system weight would positively affect endurance, but negatively affect payload capacity. To optimize our design parameters, we used the scoring rubric as a loss function to heuristically optimize for the capabilities that would maximize our competition score. The major design parameters identified were:

- Vehicle configuration
- Payload capacity
- All up weight (AUW)
- Thrust to weight ratio
- Ease of construction
- Total cost
- Repairability

- Stability
- Aerodynamic efficiency (drag)

3.2.1 Vehicle Configuration

We discuss vehicle configuration in detail as it affects all the design parameters. The following VTOL capable configuration were considered:

Single rotor: Increasing rotor diameter increases efficiency making helicopters efficient, but they are much harder to pilot unless experienced [1]. The mechanical complexity of a tail-rotor and geared main rotor also makes this configuration unappealing. A dual or contra-rotating rotor arrangement does away with the need for a tail-rotor but does not reduce mechanical complexity of the main rotor. We moved away from this configuration due to the complexity of manufacture, and the inherent safety risks of a large main rotor.

Tilt rotor: This configuration can be a pure multi-copter or one with a lifting body such as flying wing with a VTOL rotor configuration. While this configuration would maximize points for technical innovation based on the DBF rubric, we predict that it would perform poorly at the in-person fly-off since the course requires the vehicle to land at each waypoint to record a successful lap. This minimizes forward flight time, increasing time spent in the VTOL configuration. The added complexity and mass of the mechanism makes this configuration unfavorable. A lifting body such as a wing attached to a quadcopter does not confer an advantage when the short distances between waypoints is considered. The extra mass of the lifting body could be better put towards increased payload capacity.

Hexacopter/Octocopter: This configuration is preferred in heavy lift applications due to its stability, redundancy in case of motor failure, and payload capacity. But this redundancy comes at the cost of added weight and cost of components. Being limited to 6.8Kg (15lbs) for this competition, we did not require 6/8 rotors to achieve the payload requirement of 4lbs. Moreover, the single 10-minute flight limit nullifies the advantages of having increased reliability.

Quadcopter: The quadrotor configuration comes in many forms such as H-frame, X-frame, hybrid frames, etc. which signify how the motors are mounted in relation to each other as shown in Figure 4. The H-frame has the advantage of allowing cameras to be placed in line with the motors removing the propellers from the field of view. Given that this year's competition allows the use of GPS positioning, we are not reliant of vision-based localization and mapping. Hybrid frames, popular in commercially available vehicles, combine the best of both worlds but require advanced manufacturing capabilities to construct with composites.

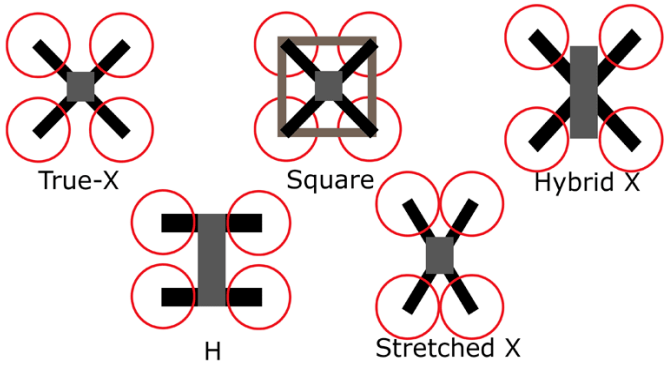

Figure 4: Various quadcopter configurations [5]

3.2.2 Scoring the configurations

We rank each of the configurations from 1 to 4 based on the design drivers identified in Section 3.2.

	Payload capacity	AUW	Thrust to Weight	Ease of construction	Total cost	Reparability	Stability	Aerodynamic efficiency	Total
Single Rotor	2	4	2	2	2	2	1	3	18
Tilt Rotor	1	1	1	1	1	1	2	4	12
Hex/Octo	4	2	4	3	3	3	4	1	24
Quad	3	4	3	4	4	4	3	2	27

The X-frame quadcopter being the structurally simplest was the design we opted as this reliable configuration is easy to manufacture, repair, cost effective, and easy to pilot.

3.2.3 Scoring onboard computation

Various vehicle components chosen were weighted based on relevant factors. For example, efficiency, max static thrust, and current draw were important design parameters for motor selection whereas, software ease of use, weight, cost, and processor speed were considerations for the onboard computing stack. Due to the page limit imposed onto this document, we show the weighting matrix for a key autonomy component, the flight controller, which demonstrates the methodology. Weights are shown in parenthesis.

	Pixhawk	ArduPilot Mega	TCMM RC 2-6s	Multiplier
Proc (MHz)	400 (3)	48 (2)	48 (2)	x4
Ease of use	(3)	(2)	(1)	x3
Weight (g)	75 (1)	31 (2)	7 (3)	x2
Cost ($)	198 (1)	49.95 (3)	91.25 (2)	x1
Total	24	21	19	
Rank	1	2	3	

4 TECHNICAL INNOVATIONS

4.1 STRUCTURAL

We make extensive use of carbon fiber (CF) tubes for our motor arms and landing legs. While a CF tube is extremely stiff, it is not straightforward to connect tubes together or to the rest of the structure. In addition, drilling a hole into a CF tube introduces defects into the epoxy-resin layer and cuts the fibers resulting in a compromised area which can fail catastrophically. We circumvent this issue by strategically reinforcing areas with aluminum alloy inserts which are bonded to the carbon fiber tube as shown in Figure 5. This also allows us to drill into the aluminum reinforced CF section without compromising its structural integrity.

We also heavily employ 3D printed components for non-structural elements such as electronics mounting brackets which allows us to rapidly prototype designs. Moreover, we used a carbon-fiber infused PLA filament for our prints which adds strength to the components with minimal increase in weight [2].

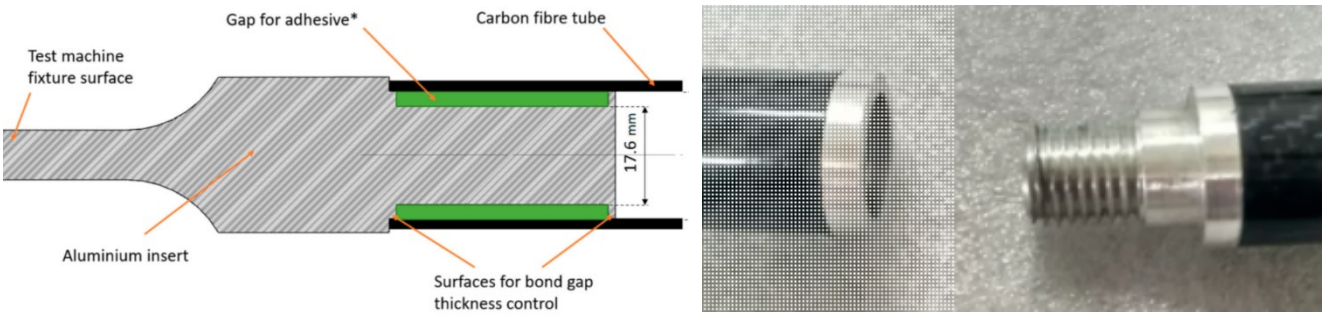

Figure 5: (left) Cross-sectional illustration of the technique used to reinforce carbon fiber rods with aluminum inserts as described in [6] (right) An example of two carbon fiber tubes with threaded inserts allowing them to be easily joined.

4.2 AUTONOMY

Localization: Originally, we proposed the use of an RTK-GPS which enabled localization to within 1cm and allowed us to rely solely on GPS for position estimates. Unfortunately, due to the limitations imposed onto the teams of not being able to use a computer manufactured in China (which comprises most consumer laptops), we would not be able to setup our RTK ground station. Our current solution uses a GPS module fused with highly accurate Z value measurements from a LiDAR ranging sensor. Based on our flight testing, our GPS module can acquire 6-10 GPS satellite signals on average and X-Y positional accuracy is sufficient to land and takeoff within the 30 ft circular VTOL zone defined in the competition.

Assisted control: We plan to assist the human pilot during the flight performance course using GPS based localization. The system will provide altitude hold and real time waypoint following capability as the GPS coordinates of the 3 landing zones is known. In practice we envision that the pilot would fly the first lap and record waypoints over the hover zone of the course. Then with the flip of a switch, the autonomous copter would automatically travel to the next way point. This guided autonomy reduces the onboard computational overhead as the pilot can instantly take back control in case of positional drift or overshoots allowing us to forgo vision entirely. Reducing pilot workload ensures our best chance of success.

4.3 MISSION MODEL

Our simulations show that for our vehicle, flying without yawing/turning the aircraft is the most effective path for the mission, i.e., keeping the nose pointed in the same direction. Assumptions we made were:

- Pilot can follow a perfectly straight line and can maintain constant velocity
- No drag and no environmental disturbances (i.e., wind gust or turbulence)
- Time to land/takeoff is not significant
- Max acceleration: 5 m/s^2
- Max speed: 15 m/s

Following equations are used to calculate the estimated time to complete the course:

$$Time\ to \max speed = \frac{abs(v_0 - v_f)}{a} = \frac{abs(-15)}{5} = 3\ sec$$

$$Distance\ covered = v_0 t + 0.5at^2 = 22.5m$$

$$dist_x = x_0 + v_{ax}t + a * \cos(\theta)\, t$$

$$dist_y = y_0 + v_{ay}t + a * \sin(\theta)t$$

$$\theta = atan2(v_{0y}, v_{0x}) or\ angle\ to\ the\ next\ waypoint$$

We compared this straight-line strategy where we come to a complete stop quickly using a maneuver popular among drone racers, *a power loop*, instead of banked turns. The length of track is 550 ft (167.6 m) and it takes 3 seconds (or 22.5 m) to reach a maximum velocity of 15 m/s.

Endurance: If we can perform a perfect run, a total of 14 laps is possible in 10 minutes. If we assume an overestimation factor of 1.5x, then, we expect to complete 9-10 laps. The main uncertainty is human performance on the day of the competition which can vary wildly for an amateur pilot.

Autonomous: Based on these parameters, we estimate to finish a lap of the course in 42.3s during a perfect run. Realistically, with an overestimation factor of 1.5x, we expect to complete a lap in 64s. Weather conditions which degrade GPS line of sight and heavy winds, or turbulence can greatly diminish autonomous flight performance and is a risk factor on the day of the competition.

5 Design Definition

5.1 Key Parameters

Max dimension in X and Y: 1043mm Max dimension in Z: 310mm CoG at (X=3.43, Y=70.89, Z=0.24) All up weight (with payload): 4.4Kg	Propeller size: 15x5.5in Max static thrust: 94.1N Max current draw: 75A	14min flight time in pure hover 16min flight time in cruise Max X/Y Velocity: 18m/s Max Z Velocity: 8m/s

5.2 Mass and Cost Breakdown

Component	Kg	Qty.	Unit Cost	Total (USD)	Description
Motors	0.68	4	46.9	187.6	SunnySky XS X3515s
ESC	0.03	1	84.99	84.99	Lumenier 60A 2-6S 4-in-1 ESC
Payload	1.81	1	25	25	4lb CanDo soft grip weights
FC	0.01	1	149.9	149.9	mRo PixRacer m15
prop	0.04	4	6.49	25.96	APC 15x5.5
Battery (Motor)	1.15	2	58.11	116.22	2x3300mah 6s 60c turnigy
Battery (Control)	0.06	1	5.09	5.09	1x1000mAh 2S 30C
RTK GPS	0.02	1	70.90	70.90	mRo GPS u-Blox Neo-M8N

Receiver	0.01	1	62.48	62.48	Futuba R617FS 2.4G
Frame	0.39	1	100	100	Custom build
Misc	0.20	1	100	100	Fasteners, wiring, etc.
All-up Weight	4.4 Kg (9.71 lbs.)		Approx. Cost	$928.14	

5.3 PROPULSION

There is a cyclic relationship between motor/battery sizing, flight times, and all-up weight (AUW). For example, increasing battery size to increase flight times results in increased AUW which in turn reduces flight time. Based on an empirical study of similarly sized vehicles commercially available, we estimated a 40% payload capacity for a flight time of 10minutes. For a 1.8Kg (4lb) payload, this meant our target AUW was 4.5Kg (10lb). A rule of thumb for performant quadcopters is a 2:1 thrust-to-weight ratio or a total thrust of 9Kg (20lb). The SunnySky XS X3515S motor was tested to produce 2.4Kg of static thrust at 100% RPM. Test results are shown in Table 3.

Table 3: SunnySky XS X3515S with 15x5.5 prop

Voltage(V)	Amps(A)	Thrust (g)	Power (W)	Efficiency (g/W)
22.2	1.9	500	42.18	11.85395922
22.2	3.4	750	75.48	9.936406995
22.2	4.9	1000	108.78	9.192866336
22.2	6.8	1250	150.96	8.280339163
22.2	8.8	1500	195.36	7.678132678
22.2	11.1	1750	246.42	7.101696291
22.2	13.6	2000	301.92	6.62427133
22.2	17.8	2400	395.16	6.07348922

Based on the component list shown in Section 4.2, we estimated the flight time in hover based on the static thrust data. We assume a max LiPo draw of 85% during which the voltage stays approximately constant at the nominal voltage of 22.2V.

$$time\ (hour) = \frac{battery\ capacity\ (Watt - hour)}{current\ draw\ (Amp)}$$

We iteratively minimized this equation by interpolating the values from Table 3 to predict motor current draw and updated the AUW as battery capacity changed based on a table of weights of commercially available 6S LiPo battery packs. We eventually converged to a battery capacity of 6600mAh (split into two 3300mAh battery packs conforming with Requirement 1.7 from Section 3.1) with an estimated AUW weight of 4.4Kg. At this weight, our estimated amp draw at hover is 20.6 Amps for an estimated hover of approximately 16.3 minutes. For forward flight we assumed a factor of 1.2 greater power consumption for a flight time of 12.4 minutes at an amp draw of 27.2 amps.

5.4 FINITE ELEMENT ANALYSIS (FEA)

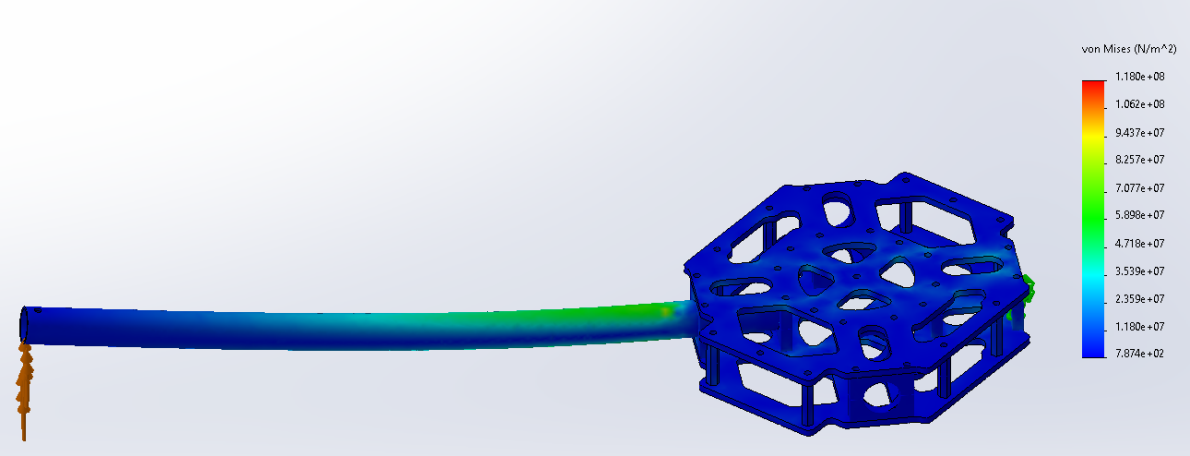

Figure 6: Full throttle static thrust simulation (top) von Mises stress distribution. Stresses are well under yield condition. The deflection at the end of the motor arm is predicted to be 4mm.

Simulations were carried out to ensure that the structure was sound under the loading condition of full static thrust with a safety factor of 1.5x shown in Figure 6. This corresponds to a loading of 40N at the end of each motor arm. These results show that we could possibly optimize the frame weight by downsizing the structural components, but this is not straightforward as many COTS components such as CF tubes, machined motor mounts, and tube clamps are not available in arbitrary sizes. Moreover, a larger margin of safety is preferred as cheap CF tubes can have varying tolerance and surface finishes.

At the scale of the aircraft we are building, commonly available raw materials (aluminum plates, CF tubes) are mass produced at certain sizing and we found that it was not worth the financial nor procurement difficulties to opt for custom cut CF frame, or thinner aluminum plates to reduce flight weight. As such the aluminum components used in our vehicle are over-engineered and we omit including detailed pictures of FEA conducted on the top and bottom 3mm aluminum plates which were both found to have a safety factor exceeding 4x.

5.5 Estimation of Aircraft Lift and Drag

We used a simplified CAD model of our quadcopter to estimate lift and drag. Conventionally, in order to measure lift and drag of an aircraft, wind tunnel tests can be used. However, due to cost and efficiency estimation, our team decided to perform CFD. The CAD model we used includes large scale bluff bodies only. Several assumptions are made to perform a CFD through SolidWorks and list of assumptions are:

- Standard temperature and pressure
- Humidity of 60%
- Gravitational inertia effects
- Turbulent and laminar flow
- Rotational flow tube around the motors
- Ambient far-field conditions
- A computational domain at least 5x diameter
- The quadcopter ‘flying’ at 10m/s at an angle of attack of -30deg

The flow through the propellers was included in the CFD figure to introduce rotational flow field conditions and vortices. Since the landing gear has negligible effect on drag compared to the rest of the body, it is

not included in this CFD model. Our preliminary results indicate a drag of 1.5N in the horizontal direction. The drag coefficient of the aircraft is calculated from the equation:

$$C_d = \frac{F_d}{0.5\rho v^2 A} = 1.45$$

Compared to a simple cylindrical bluff body with a coefficient of drag of 1.24 at flow velocity of 1.75m/s, the calculated C_d could be underestimated. Since a simplified CAD model was used and a mesh refinement study was not conducted, the drag coefficient of 1.45 needs further validation.

5.6 Stability – PID Tuning

Stability is the ability of an aircraft to return to its initial state when a disturbance such as turbulence or flight control inputs acts on it. Unlike fixed wing aircraft, our multirotor is statically and dynamically unstable meaning that when its attitude is perturbed there will divergent behavior. For example, if the aircraft starts rolling due to an external force, this roll angle would keep on increasing. To maintain control, a flight controller constantly monitors the aircrafts attitude and controls the RPM of the rotors to maintain commanded roll, pitch, and yaw values and rates respectively. This is accomplished using PID controllers.

The PID controller is so named because its output is a sum of three terms: a proportional, an integral and a derivative term. Each of these terms is dependent on the error (S_V – P_V) between the input and the output where S_V is the Set-Point, P_V is the process variable. This error is used to generate control signals which try to minimize the error such that the vehicle attains the set-point values.

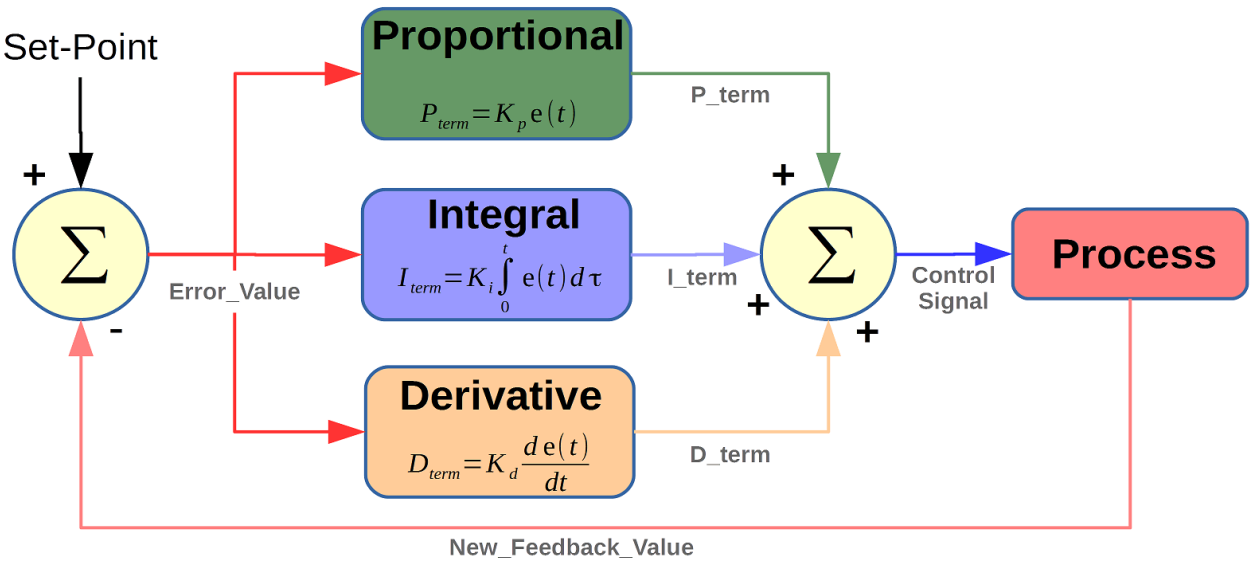

Ill tuned PID controllers can result in unstable or oscillatory behavior manifesting as the vehicle overshooting and then undershooting the set-point value continuously in a stable or divergent manner leading to loss of control. Adjusting each of the terms has the following effect:

Proportional term (Pterm): This term speeds up the response as the closed loop time constant decreases with the proportional term. It also minimizes but does not eliminate the steady state error, or offset.

Integral term (Iterm): Eliminates the offset and increases the system response speed. But it can cause oscillation in the system.

Derivative term (Dterm): This term primarily reduces the oscillatory response of the system but also can drive it unstable quickly.

A change in the proportionality constants of these terms changes the type of response for the system. That is why PID tuning, which is the variation of PID proportionality constants is of the utmost importance. The goal of tuning is to ensure minimal process oscillation around the setpoint after a disturbance has occurred which improves the overall performance. We started with a low proportional gain, with integral and derivative terms disabled. Then we adjusted the value of the 3 terms in a sequential manner by following the steps below:

- Modify the gain while looking at the controller response to a step input
- Continue adjusting gain until the vehicle attitude can achieve the step input setpoint

Our PID analysis from flight logs showed that its movement is almost exactly matching to the expected behavior. We have tested the input noises from vibration of the vehicle frame during the flight and minimized the vibration by adding dampers on the casing for flight controller and GPS modules.

6 Dimensional Drawings

Figure 7 and Figure 8 show relevant dimensions of the vehicle design using the top, side, and front views respectively.

All dimensions are specified in millimeters. Units have been omitted on the drawings to increase readability. The drawings have a scale of 1:5.

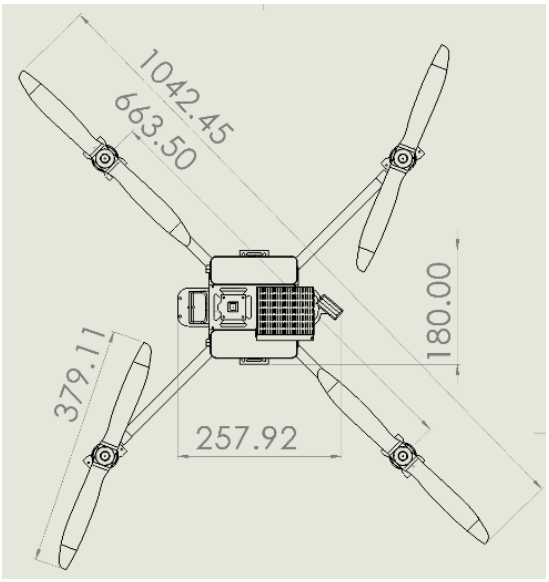

Figure 7: Top view confirming that the vehicle conforms to the sizing restrictions

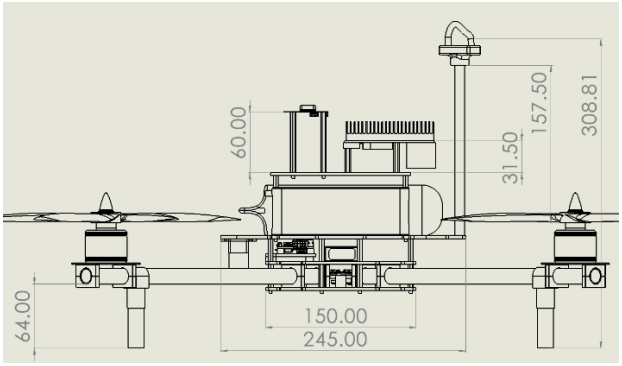

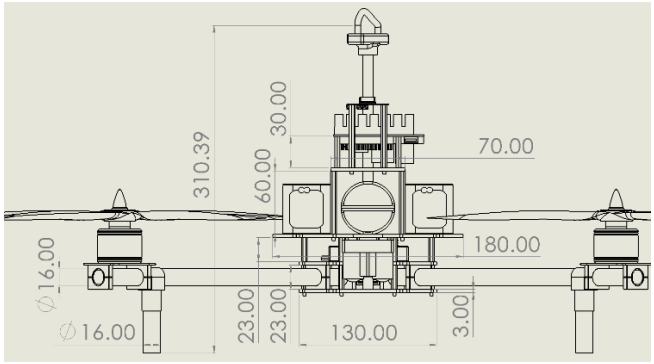

Figure 8 (left) Side view of vehicle (right) Front view of vehicle

6.1 ELECTRONICS

Figure 9 shows a block diagram of the electronics subsystem with the communication protocol highlighted in green. Wireless links are denoted with dashed lines. The ground station is a mobile phone conforming to the country of manufacture regulation imposed upon the teams.

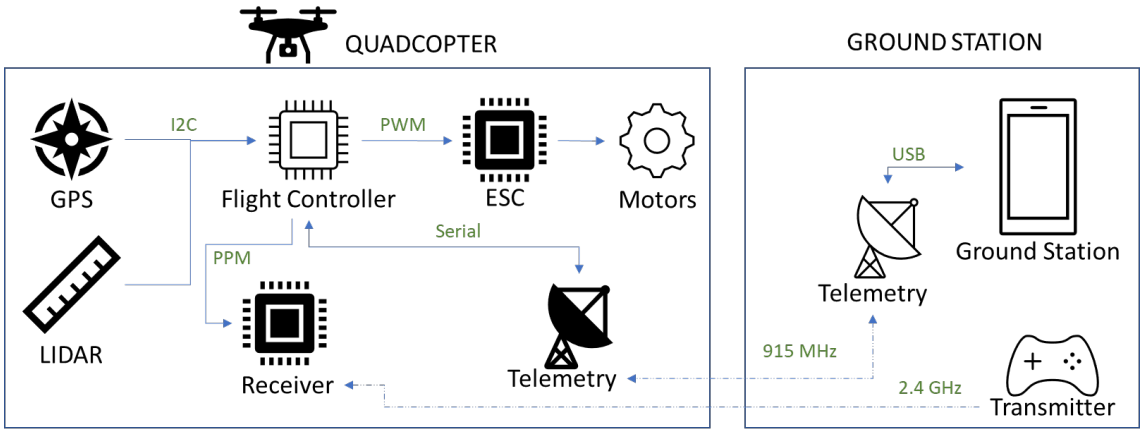

Figure 9: Block diagram of electronics and communication protocol between sub-systems

6.2 CAD MODEL

Figure 11 and Figure 10 shows the various components visible when the vehicle is viewed from the front and side respectively.

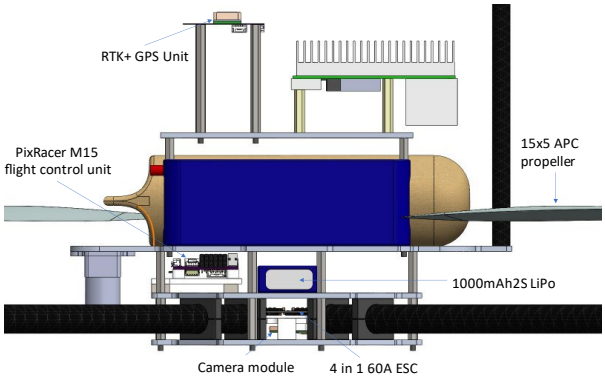

Figure 10: Side view of CAD model

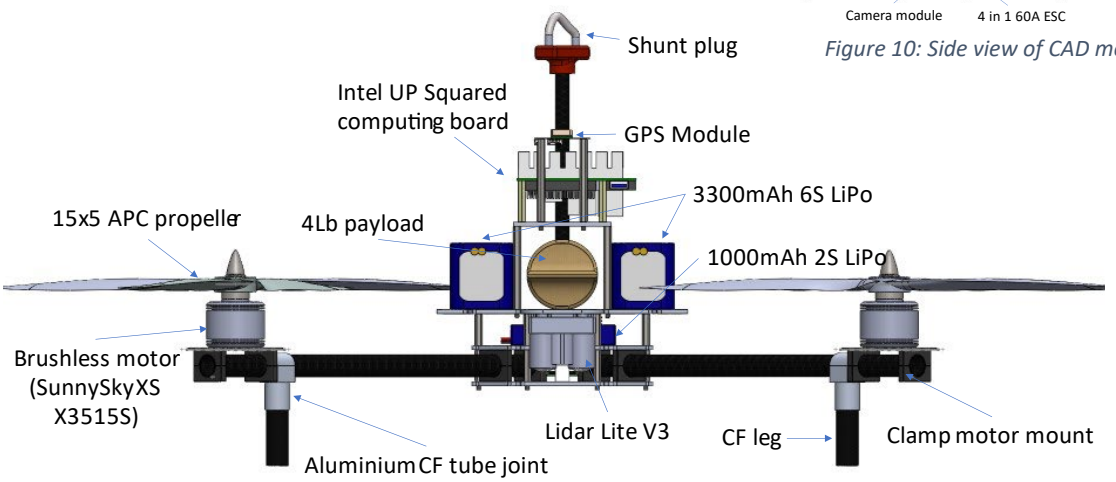

Figure 11: Front view of CAD model

7 FABRICATION:

The manufacturing processes available to the team were a lathe, mill, CNC router and a 3D printer. The main driver of the manufacturing process was material selection, health and safety considerations, and prior machining experience. Carbon fiber and aluminium have been proven time and time again to be the best choices for the construction of quadcopter under 50lbs. Carbon fiber plates are widely used in the industry for the manufacture of quadcopters but machining them poses serious health risks due to the carcinogenic nature of carbon dust prompting the use of aluminium plates in their stead for our custom frame. We chose to work exclusively with the 6061-T6 and 7075 aluminium alloys due to their machinability. The main downside of 3D printed components is their weakness in directions that are perpendicular to the layers due to delamination. This can be overcome through careful design that ensure that the part is loaded parallel to the layers. Moreover, the strength of the components was improved using carbon fiber reinforced PLA for 3D printed components.

8 TESTING

We conducted flight tests to validate the hover and cruise flight times, manual lap time, autonomous lap time, and structural integrity of the vehicle.

8.1.1 Flight Time Validation

We manually flew the aircraft to determine flight time until the low battery warning was triggered or until the human pilot experienced loss of motor power leading to a decision to land. We found that our cruise flight time was 16.5 minutes (landed due to low battery warning) and pure hover flight time was approximately 14 minutes (loss of motor power along with low battery warning). Our theoretical model in Section 5.3 over-estimated the hover flight time whereas it under-estimated the cruise flight time. This increased cruise flight time as compared to hover flight time which was contradictory to our theoretical model's assumption can be explained by recent research which shows that minimum power consumption occurs at forward flight rather than hover for simple spherical geometries [3].

8.1.2 Experimental mission profile/performance

The mission profile table is based off a test flight carrying a 4 lbs. CanDo soft grip payload in autonomous mode as it is repeatable compared to manual flight. The table below shows power consumption, time, speed, and distance for each maneuver. We limited the descent rate to reduce stresses on the frame during landing. The table below shows the best obtained mission profile over the single run of the full course in autonomous mode.

	Takeoff	**Cruise**	**Landing**	**Standby**
Avg Power	600 W	530 W	480 W	< 5 W
Time	16 s	134 s	18 s	N/A
Speed Limit	3 m/s (9.8 ft/s)	5 m/s (49.2 ft/s)	1 m/s (3.3 ft/s)	0 m/s
Distance	6m (20 ft)	435m (1420 ft)	6m (20 ft)	N/A

As the flight speed does not affect scoring for the autonomy course, we lowered the max allowable X and Y velocity to 5 m/s as this greatly increases our safety margin.

8.1.3 Manual Flight

Our pilot is an amateur drone enthusiast and understandably is unable to push the vehicle to its max flight velocity and consistently maintain such high speeds. On average it takes 1 to 1.5 minutes for our pilot to complete each lap resulting in 6-10 laps. This is much lower than our predicted best-case scenario of 14 laps in Section 4.3. We hope this is improved with continued flight training.

8.1.4 PID Controller Performance

Figure 12 shows the step response of the yaw rate, roll angle, roll rate, and pitch rate PID controller estimated from our flight test data. We see the need for a higher proportional value in general due to the slow response time of the quad. While this prevents overshoots, it leads to a 'sluggish' feeling vehicle which our pilot does not prefer. The pitch rate on the other hand might benefit from an increased damping value as oscillations are present after the overshoot unlike the roll rate which is adequately damped. This illustrates how the team is using flight log data to tune the stability characteristics of the quadcopter.

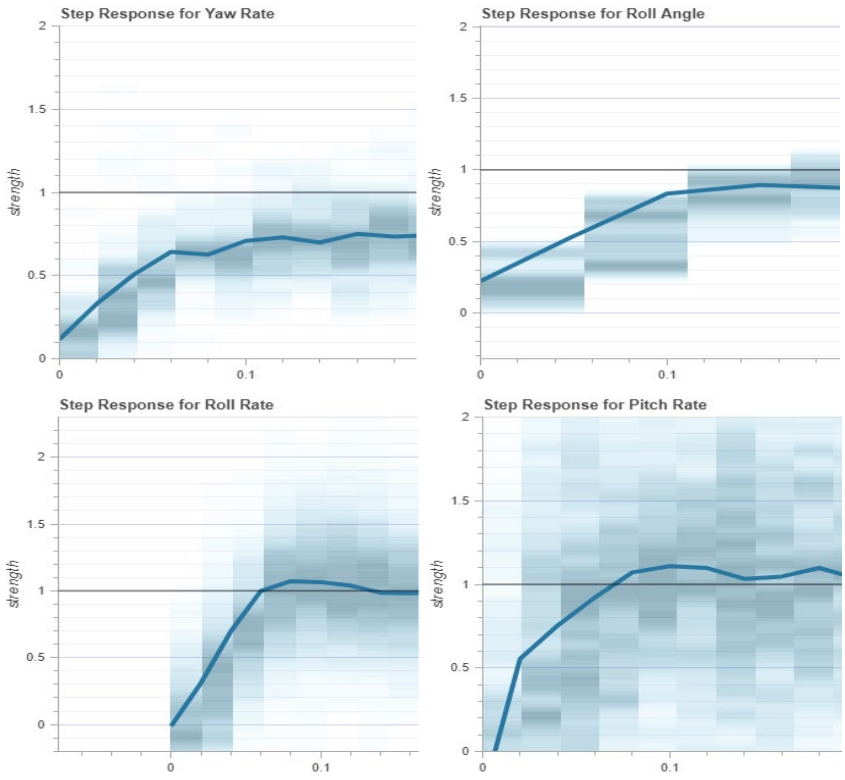

Figure 12: Graphs showing the step response of the PID controllers

9 Works Cited

[1] G. J. Leishman, "Disk Loading and Power Loading: Principles of helicopter aerodynamics," in Fundamentals *of Rotor Aerodynamics*, Cambridge university press, 2006.

[2] N. Maqsood and M. Rimašauskas, "Characterization of carbon fiber reinforced PLA composites manufactured," *Composites Part C: Open Access,* vol. 4, 2021.

[3] B. Theys and J. D. Schutter, "Forward flight tests of a quadcopter unmanned aerial vehicle with various spherical body diameters," *International journal of micro air vehicles,* vol. 12, 2020.

[4] Vertical Flight Society, "VFS," 16 12 2021. [Online]. Available: https://vtol.org/files/dmfile/rfp-2022_vfs-dbvf_final-5.0_16dec2021.pdf.

[5] Dronenodes, "Dronenodes," 2018. [Online]. Available: https://dronenodes.com/wp-content/uploads/2018/12/quadcopter-frame-shapes.png.

[6] W. Rządkowski , J. Tracz, A. Cisowski, K. Gardyjas, H. Groen, M. Palka and M. Kowalik, "Evaluation of Bonding Gap Control Methods for an Epoxy Adhesive Joint of Carbon Fiber Tubes and Aluminum Alloy Inserts," *Materials,* vol. 14(8), no. Adhesive Bonding Lightweight Materials in Modern Vehicles Construction, p. 1977, 2021.